Tailored "Sandwich" Strategy in Surface Enhanced Raman Scattering: Case Study with para-Phenylenediamine and Application in Femtomolar Detection of Melamine

ARTICLE *in* THE JOURNAL OF PHYSICAL CHEMISTRY C · NOVEMBER 2014

Impact Factor: 4.77 · DOI: 10.1021/jp5111955

3 AUTHORS, INCLUDING:

Soumen Dutta
IIT Kharagpur
20 PUBLICATIONS **116** CITATIONS
SEE PROFILE

Tarasankar Pal
IIT Kharagpur
252 PUBLICATIONS **8,548** CITATIONS
SEE PROFILE

THE JOURNAL OF PHYSICAL CHEMISTRY C

Article

pubs.acs.org/JPCC

Tailored "Sandwich" Strategy in Surface Enhanced Raman Scattering: Case Study with *para*-Phenylenediamine and Application in Femtomolar Detection of Melamine

Sougata Sarkar, Soumen Dutta, and Tarasankar Pal*

Department of Chemistry, Indian Institute of Technology, Kharagpur-721302, India

Supporting Information

ABSTRACT: Herein, we have implemented a modified sandwich strategy for surface enhanced Raman scattering (SERS) studies aimed at the accomplishment of remarkably enhanced vibrational signatures from preferred Raman probes. Here, *para*-phenylenediamine (or PDA) has been selected as the test molecule which can concurrently bind to two metal surfaces with its two terminal amino ($-NH_2$) groups. We have deliberately placed this molecule in the nanogaps found in between a nanostructured silver film/island and gold core−silver shell nanoparticles using a tailormade approach. The whole method of fabrication of this sandwich-type assembly follows a simple colloidal chemistry route. We observed highly enhanced and well resolved Raman signals from the PDA molecule in this sandwich (i.e., nanostructured Ag-film@PDA@Au_c-Ag_s) assembly. The spectral characteristics were also compared with other modes of assembly/association of the molecule in different Raman active plasmonic environments, and from all these comparative outcomes, we reach the conclusion that this particular sandwich assembly offers the most enhanced SERS profiles for the molecule. It is believed that the generation of immense numbers of SERS active hot spots in the nanogaps of the sandwich assembly cause an exceedingly enhanced electromagnetic field which principally contributes in the observed enhancement. A comparative SERS study was also made with different excitation wavelengths (632.8 and 514 nm lasers, respectively). Finally, we employed this SERS active sandwich-based plasmonic platform for the analytical assay of a common infant and milk-product contaminant, melamine. For this, we have chosen melamine as the Raman probe instead of PDA and have designed a similar sandwich assembly. Then we carried out SERS measurements of melamine employing this sandwich assembly (nanostructured Ag-film@melamine@Au_c-Ag_s). The SERS spectrum was individually recorded for four different concentrations of melamine, and ultimately we were able to detect its concentration down to the femtomolar level (i.e., limit of detection = 10^{-15} M). Thus, the tailored sandwich-based SERS strategy offers a simple roadmap toward the achievement of highly enhanced SERS signatures from molecules even at trace level concentrations.

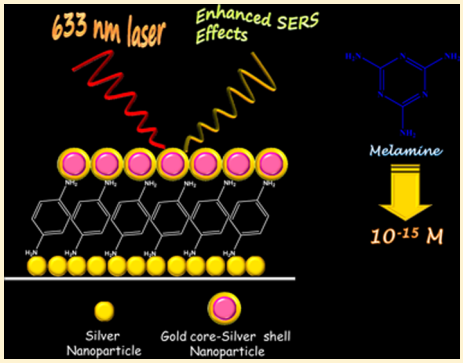

INTRODUCTION

In situ Raman studies of most adsorbates are limited by their very low intensity profiles owing to its smaller cross section compared to that of infrared and fluorescence cross sections, and thus, after its inception by Fleischman et al. in 1974,[1] surface-enhanced Raman scattering (SERS) has been exploited to boost the detection sensitivity enormously. Though the origin of enhancement in SERS is still not fully understood, these days it is absolutely believed that the observed enhancement is primarily contributed by two mechanisms: a long-range electromagnetic effect where, at or near laser-irradiated noble metal particle surfaces, local electromagnetic field is enhanced as a result of localized surface plasmon excitation, leading to more intense Raman scattering from molecules near or adsorbed onto the particle surfaces; and a short-range chemical effect which involves specific interactions or coupling between the molecule and the metal particles.[2,3] Subsequently, this spectroscopic technique has also enlightened the study on the vibrational natures and spatial orientations of adsorbed molecules at metal−adsorbate surfaces and interfaces.

The past decades have witnessed numerous true attempts made to fabricate a variety of different SERS active nanostructures.[4] At their nanoscale, noble/coinage metals are the most prescribed substrates to enhance SERS, though some endeavors with so-called "ill-defined" SERS active transition metal nanoparticles have also been successfully accomplished.[5,6] SERS has also been achieved from a combined platform of noble metal and transition metal nanostructures.[7,8] The foremost aim of all these attempts is to enrich the electromagnetic and/or chemical enhancement contributions to produce satisfactory SERS spectral features. In this connection, the introduction of a new recipe, defined as a "sandwich strategy", by different research groups, in the achievement of enhanced SERS signatures, is worth mentioning.[9−13] Kim's group has made an assortment of significant contributions to this strategy:[14−20] this approach involves the trapping of molecules between two noble metal platforms in a

Received: November 8, 2014

   dx.doi.org/10.1021/jp5111955 | J. Phys. Chem. C XXXX, XXX, XXX−XXX

sandwich fashion. Either one or both of these platforms may be in a nanoregime.[14−20] It is anticipated that the gigantic electromagnetic enhancement in this sandwich-like metal−molecule−metal junction results either from coupling of localized surface plasmons (LSP) when both of the two metals are nanodimensionl or from the coupling of localized surface plasmons of the nanostructured metal with the surface plasmon polariton (SPP) of the macroscopic metal surface.[9−20] The observed enhancement has also been supported by theoretical calculations.[16,18] The variety of homometallic (both platforms are of same metal) and heterometallic combinations have been exemplified in this concern, though in all these cases, each of the metallic platforms is of pure metallic nature. Very recently, gold/silver alloy nanoparticles have been introduced in lieu of individual metallic nanoparticles.[20] This leaves introduction of other hybrid nanostructures such as core−shell nanoparticles as one of the components for configuring the sandwich arrangement.

This spectroscopic method, being rapid and nondestructive, shows a reliable sensitivity toward different analytical assays, for instance, in biomolecular sensing, in detection of polyaromatic hydrocarbons (PAHs), explosives, food contaminants, and heavy metal ions/anions, and so on.[21−26] Melamine is a common organic raw material for large scale industrial production of melamine resin, an extensively used thermostable polymer for manufacturing a variety of commercial products like kitchenware, plastics, and filters. It is also well-known as an adulterant in milk products (e.g., infant formula) to supplement their apparent protein content with its rich nitrogen content (66% by mass). Such adulteration can cause acute renal disease and even infant death, so this has prompted the restriction of melamine to a maximum limit of 2.5 ppm in food products and 1 ppm in infant formula by both United States and China Governments. Therefore, rapid detection of melamine is a highly challenging task and different analytical measurements have been carefully executed to solve this challenge.[27−36] SERS is one of the widely accepted spectroscopic tools for rapid, sensitive, accurate, and real time detection of melamine.[37−46]

The present study describes the implementation of a tailored sandwich-based SERS strategy using silver nanoparticle film and gold core−silver shell (Au_c-Ag_s) nanoparticles as the SERS active plasmonic substrates. We have first chosen *para*-phenylenediamine (PDA) as the Raman probe and examined its SERS spectral characteristics in different environments, such as PDA attached (i) on only silver nanoparticles film (i.e., SERS from Ag@PDA); (ii) in sandwich arrangement between nanostructured silver film and Au_c-Ag_s nanoparticles (i.e., SERS from Ag@PDA@Au_c-Ag_s); (iii) in sandwich arrangement between nanostructured silver film and Ag nanoparticles (i.e., SERS from Ag@PDA@Ag); (iv) on only Au_c-Ag_s nanoparticles (i.e., SERS from Au_c-Ag_s@PDA). We observed that maximum enhancement of Raman signals occurs when PDA is located in between nanostructured silver film and Au_c-Ag_s nanoparticles in a sandwich fashion. The spectral bands are also discrete in nature and well resolved. It is anticipated that the SERS active hot-spots produced in the nanogaps, formed between the nanostructured Ag island and Au_c-Ag_s nanoparticles, are responsible for the enormous SERS enhancement in this specific sandwich mode (i.e., Ag@PDA@Au_c-Ag_s). The superior enhancement results from the gigantic contribution from the electromagnetic field generated in the above nanogaps. We have also studied the time-dependent kinetics of the above SERS measurement from the Ag@PDA@Au_c-Ag_s assembly. Again, we have performed the sandwich-based SERS study of PDA replacing the nanostructured Ag film with a mechanically polished, thoroughly washed and cleaned silver foil (i.e., SERS from Ag foil@PDA@Au_c-Ag_s in-place of Ag@PDA@Au_c-Ag_s), and we observed an identical spectral pattern of the molecule to that of the SERS pattern from the Ag@PDA@Au_c-Ag_s assembly but with much lower intensity enhancement. Therefore, we have concluded that the sandwich assembly made with nanostructured Ag film and Au_c-Ag_s nanoparticles provides an advantageous avenue to achieve a prominent SERS effect. Finally, we have implemented the SERS active sandwich-based plasmonic platform in the analytical assay of melamine. Melamine has been used as the Raman probe in lieu of PDA in the above sandwich assembly, and prolific SERS enhancement has been achieved from this molecule, and finally, with this strategy we were able to detect melamine concentration down to the femtomolar (10^{-15} M) level. Thus, such low-level detection of melamine has been achieved here with our designed SERS active sandwich architect. Thus, the recipe offers high promise of trace level detection of different food adulterants and other contaminants also.

EXPERIMENTAL SECTION

All the reagents used were of AR grade and used as received without further purification. Methanol, acetone, sodium hydroxide, 30% H_2O_2, and 98% H_2SO_4 were purchased from Merck, India. Triton X-100 [$(C_{14}H_{22}O(C_2H_4O)_n)$, polyethylene glycol *p*-(1,1,3,3-tetramethylbutyl)-phenyl ether; TX-100], cetyltrimethylammonium bromide (CTAB), ascorbic acid, silver nitrate ($AgNO_3$), chloroauric acid trihydrate ($HAuCl_4{\cdot}3H_2O$), and *para*-phenylenediamine ($C_6H_8N_2$) were purchased from Aldrich. Glassware was cleaned using aqua regia, subsequently rinsed with a copious amount of double-distilled water, and dried well prior to use.

The gold core−silver shell nanoparticles were synthesized following a published method by Liz-Marzán et al.[47] In brief, a gold colloid of ∼20 nm spherical nanoparticles was synthesized using the standard Frens's method.[48] Then, to 20 mL of a 50 mM aqueous solution of CTAB, 1 mL of 0.1 M ascorbic acid solution, 0.5 mL of 10 mM $AgNO_3$ solution, and 0.5 mL of the as-synthesized citrate stabilized Au colloid were sequentially added. Finally, to this solution, 0.1 mL of 1.0 M NaOH solution was added in a dropwise fashion and slowly mixed through gentle shaking. A fast color change from red to yellow indicates the formation of gold core−silver shell nanoparticles having approximately uniform diameter of 45−50 nm (Supporting Information Figure S1).

Microscopic glass slides were sonicated with 1:1 mixture of acetone and methanol for 20 min to remove the contaminants and, then, thoroughly washed with double-distilled water. The slides were then immersed in freshly prepared "piranha" solution (70% H_2SO_4 + 30% H_2O_2) at room temperature for 30 min (*Caution: This mixture reacts violently with organic materials and must be handled with extreme care!!!*). After the "piranha" wash, the glass slides were cleaned with copious amounts of highly pure water and dried under vacuum. Glass slides treated in this way were enriched with surface hydroxyl groups. Then, these glass slides were further treated with 1 M NaOH solution at 85 °C for 2 h, subsequently thoroughly rinsed with double distilled water and dried again at 60 °C under vacuum.

dx.doi.org/10.1021/jp5111955 | J. Phys. Chem. C XXXX, XXX, XXX−XXX

Five milliliters of a 1 M aqueous $AgNO_3$ solution was stirred with 1 mL of 0.05 M Triton X-100 solution in a 50 mL beaker for 2 h in the dark. The freshly modified glass slide was then immersed in the above solution and exposed to UV-irradiation (365 nm) in a 15 mL glass vial for a predetermined period of time. Silver nanoparticles were deposited on the slide. Then, the slide was thoroughly rinsed with double-distilled water to remove any unbound ions or surfactant molecules. The slide was then incubated in 10^{-6} M ethanolic solution of *p*-phenylenediamine (abbreviated as PDA hereafter) overnight, and SERS was recorded from this PDA assembled silver film (referred to as Ag@PDA).

The above film (Ag@PDA) was incubated in the Au_c-Ag_s sol for a predetermined period of time to ensure adsorption of Au-core@Ag-shell (Au_c-Ag_s) nanoparticles onto the pendent NH_2 groups (as the other NH_2 groups already remain anchored over the Ag nanoparticles). The final sandwich arrangement obtained in this way could be denoted as Ag@PDA@Au_c-Ag_s and SERS study was performed on this arrangement. SERS studies were also performed on Au_c-Ag_s@PDA, Ag@PDA@Ag, and Ag-foil@PDA@Au_c-Ag_s assemblies for comparative SERS data.

We have used melamine (at varied concentrations) in lieu of PDA in the sandwich arrangement, and SERS study was performed to determine the presence of melamine spectroscopically. For each case, we first fabricated the silver film over the glass slide, then incubated the film in melamine solution, followed by further incubation of the melamine anchored film in the gold core−silver shell colloid. We then recorded the SERS spectra. For the different concentrations of melamine as described in the MS (four sets: 10^{-5}, 10^{-8}, 10^{-10}, and 10^{-15} M, respectively), the experiment was performed for each concentration of melamine with freshly prepared silver film and fresh core−shell nanocolloid.

RESULTS AND DISCUSSION

Fabrication of Nanostructured Silver Film on Glass Substrate. Photochemical reduction reaction is a common practice in colloidal chemistry for greener synthesis of noble metal nanoparticles/nanostructures.[49] Here we have employed Triton X-100 (TX-100) to act as a free-radical source upon photoexcitation. These radical ions could carry out smooth reduction of the silver ions. Again, TX-100, being a well-known nonionic surfactant, simultaneously controls the size of the photo-produced silver nanoparticles.[50] These nanoparticles are subsequently deposited on glass substrates. Figure 1a presents the FESEM image of the as-synthesized Ag film which clearly suggests complete coverage of the glass surface with the deposited nanoparticles. We also observed colonial growth of the nanoparticles throughout the film resulting from the simultaneous reduction and overgrowth of the nanoparticles upon the primarily formed nanoparticle layer. Mostly, the nanoparticles were spherically shaped and remained closely associated, resulting in a macroscopically rough surface. The bumpy growth of the nanoparticles is also evident from the corresponding tapping mode AFM image (Figure 1b). Here it is important to note that the measurement of size of individual particles was quite impossible, as the particles coalesced with each other and their boundaries vanished or appeared blurred. Again, from TEM analysis (inset of Figure 1a) of the as-synthesized Ag nanoparticles, we observe that maximum numbers of the particles have diameters of ~50 nm, although diameters range from 20 to 50 nm and it is also clear that most

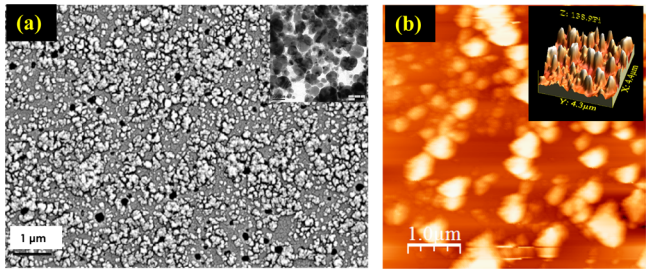

Figure 1. (a) FESEM image of the nanostructured silver film deposited on the glass substrate (Inset: TEM image of the silver nanoparticles) [Conditions: The freshly modified glass slide was immersed in a solution mixture of 5 mL 1 M aqueous $AgNO_3$ solution and 1 mL 0.05 M TX-100 solution and exposed to 365 nm UV-irradiation]. (b) AFM image (face projection) of the silver film (inset showing the height projection of the deposited film).

of the particles coalesce with each other. The elemental mapping and EDX analysis clearly demonstrate the presence of silver nanoparticles over the entire glass surface (Supporting Information Figures S1 and S2).

Normal Raman Scattering of *para*-Phenylenediamine. The normal Raman scattering (NRS) spectrum of PDA in solid state is presented in Figure 2a. The molecule, PDA, shows C_1 symmetry in its optimized molecular geometry and has a total of 42 vibrations. The strong 1618 cm^{-1} band has been assigned to 70% ring deformation (C−C stretching) mode as described from the potential energy distribution (PED) calculations.[51] Similarly, *p*-CN stretching (31%), ring breathing (29%), and ring-N stretching (27%) contribute to the strong band at 1266 cm^{-1}. The most intense spectral line is observed at 845 cm^{-1} which has been prescribed to have maximum contribution from ring breathing mode (62%) and less contribution from 14% ring deformation. Here it is worth mentioning that, for the other two isomers of phenylenediamine (ortho- and meta-), the most intense bands appear at 1033 (30% ring breathing and 32% ring deformation) and 989 cm^{-1} (38% ring breathing and 59% ring deformation), respectively. This positional shift of vibrational mode with different extent of contribution from ring breathing for the three isomers clearly indicates the sensitivity of this mode toward the position of the second NH_2 group in the phenylenediamine moiety. Again, the 648 and 473 cm^{-1} bands have been assigned primarily to ring deformation modes. Similarly, the Raman signature in the low frequency region, 368 cm^{-1}, appears from ring deformation and ring-CH wagging modes.

Surface Enhanced Raman Scattering of *para*-Phenylenediamine over the Silver Film. On the as-formed silver film incubated in 10^{-6} M ethanolic solution of PDA overnight, we observed an enhanced Raman spectrum of the molecule (Figure 2b) though no Raman spectrum was obtained from only 10^{-6} M ethanolic solution of PDA. The SERS spectrum was distinctly different from the NRS spectrum. Here it is worth mentioning that this difference primarily occurs from the formation of *para*-phenylenediamine radical cation ($PDA^{+\cdot}$) in solution whereas in the solid state no such ion formation takes place.[52] Therefore, Figure 2b actually represents the SERS spectrum of the existing radical ion in solution over the nano silver island.

The 1630 cm^{-1} band arises from the in-phase combination between δNH_2 (scissor) and C═C stretching vibrations with nearly equal contributions from both of them. This mode is also observed in the FTIR spectrum of PDA, but as expected

dx.doi.org/10.1021/jp5111955 | J. Phys. Chem. C XXXX, XXX, XXX−XXX

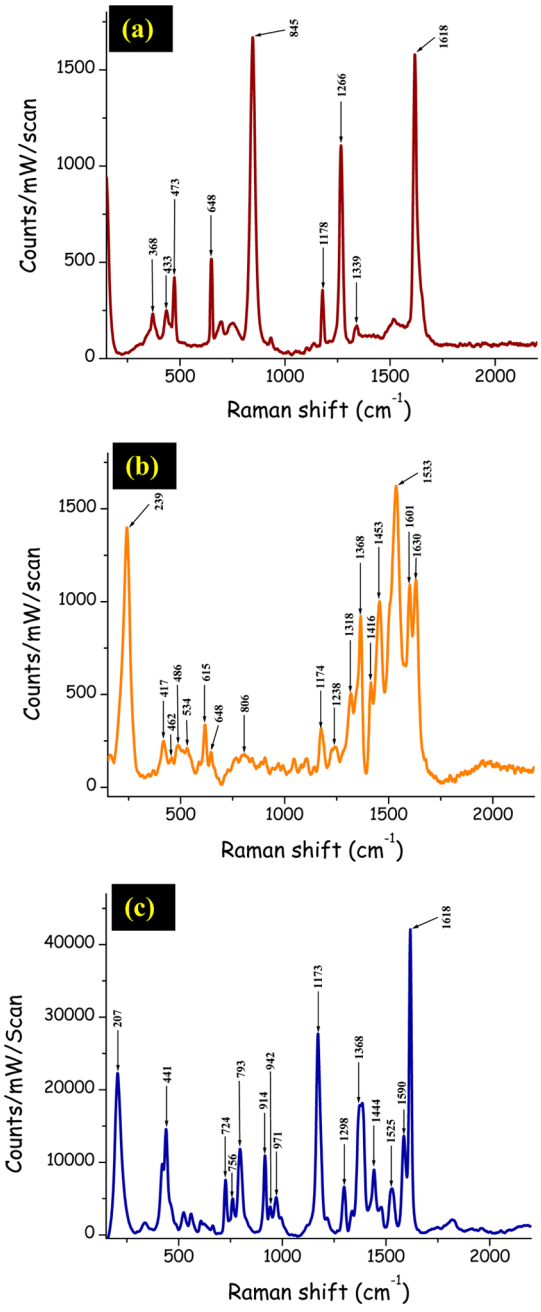

Figure 2. (a) Normal Raman scattering spectrum of *para*-phenylenediamine (PDA) in solid state. Surface enhanced Raman scattering spectrum of PDA (10^{-6} M) (b) on the nanostructured silver film deposited on glass substrate and (c) in sandwich mode, i.e., when the PDA molecule remains trapped between the silver film and gold core–silver shell nanoparticles (i.e., SERS from Ag film@PDA@Au_c-Ag_s assembly).

this IR-active mode should not appear in the Raman spectrum as both the PDA and $PDA^{+\cdot}$ have D_{2h} symmetry. It could be anticipated that, upon coordination with the metal surface, the loss of molecular symmetry allows the observation of this IR-active mode in the SERS spectrum. The 1601 cm^{-1} band in the SERS spectrum is principally assigned to the ring deformation (C–C stretching) mode, but a relative drop in intensity is observed compared to its NRS counterpart at 1618 cm^{-1}. This result could be interpreted from surface selection rules for SERS, which explain the enhancement of the normal modes of vibrations having components perpendicular to the surface of the substrate. Thus, the above decrease in intensity indicates the tilted orientation of the molecule relative to the surface. The highest intense SERS band at 1533 cm^{-1} is predominantly assigned to the CN stretching mode (both coordinated and noncoordinated) suggesting the NH_2 group as the adsorption site. The above frequency is in between the characteristic values of C═N (~1600 cm^{-1}) and C—N (~1200 cm^{-1}) stretching vibrations pointing toward the CN bond order of ~1.5. This is analogous to the CO stretching frequency observed in the *p*-benzosemiquinone anion and hydroquinone cation radicals. Another enhanced signal arises at 1453 cm^{-1} which has no signature in the NRS counterpart. Similarly, the weak bands at 534 and 486 cm^{-1} indicate the stretching of MN and bending of MNC vibrations. We also noticed the appearance of a new band at 417 cm^{-1}. The strong band at 239 cm^{-1} is the distinct signature of formation of the M–N (or Ag–N) bond. Here it is worth noting that the highest intensity NRS band at 845 cm^{-1} is absent in the SERS spectrum which is presumably caused by the coordination driven loss of molecular symmetry. Therefore, these vibrations indicate the attachment of the PDA molecules upon the nanostructured silver surface. Similarly, the other vibrational modes could also be explained.

Surface Enhanced Raman Scattering of *para*-Phenylenediamine Sandwiched between Nanostructured Silver Film and Gold Core–Silver Shell Nanoparticles: Mechanistic Overview and Comparative Study. We incubated the PDA assembled silver film in Au_c-Ag_s sol for a predetermined period of time to achieve a sandwich arrangement of the PDA molecule where the pendant amino groups of the molecules will now attach to the surface of the core–shell nanoparticles. We would now have PDA molecules trapped within the nanostructured silver film and the Au_c-Ag_s nanoparticles likewise in a sandwich fashion. When we look at the SERS spectrum obtained from this sandwich substrate, we surprisingly noticed that the SERS pattern differs from the first-recorded SERS spectrum (i.e., PDA assembled on silver surface; Ag@PDA) with surprising enhancement of Raman signals (Figure 2c). For example, from this figure (i.e., from Figure 2c) we observe that the 1618 cm^{-1} band is the highest-intensity Raman signal in the spectral window. This band was also the most intense in the NRS spectrum of PDA, but in the first-recorded SERS window, there was a weak signature of this mode at 1601 cm^{-1}. We also observed the other enhanced/new bands appearing at 1173, 914, 793,756, and 441 cm^{-1} in the sandwich structure.

Going through the literature[52] and from the above three spectral profiles, we finally notice that, in the first-recorded SERS spectrum (i.e., SERS from Ag@PDA), the more enhanced modes are principally not totally symmetric vibrations (b-type) while in the case of sandwich recipe (i.e., SERS from Ag@PDA@Au_c-Ag_s), the preferentially enhanced bands (e.g., 1618, 1173, 914 cm^{-1}) are totally symmetric vibrational modes (a-type). These totally symmetric modes are in-plane in nature. It is anticipated from the surface selection rule[53,54] that favorable appearance of totally symmetric in-plane modes (a-type) are caused by leading participation of electromagnetic (EM) enhancement mechanism in SERS, while the not totally symmetric b-type modes are enhanced by the involvement of a chemical (CE) enhancement mechanism.

This observation clearly indicates that the nanogap formed upon the attachment of Au_c-Ag_s nanoparticles in our sandwich

dx.doi.org/10.1021/jp5111955 | J. Phys. Chem. C XXXX, XXX, XXX–XXX

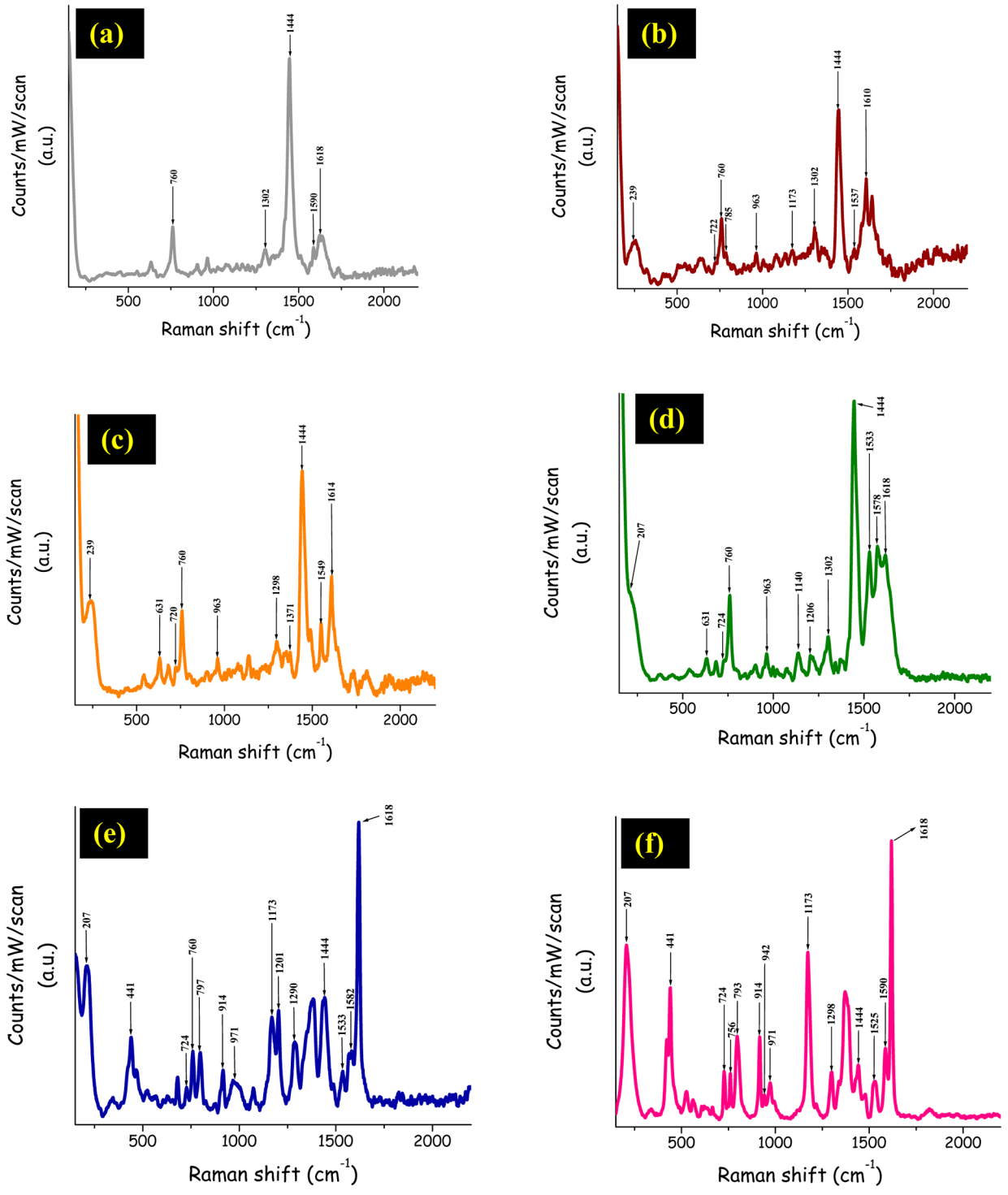

Figure 3. (a–f) Time-resolved SERS spectra of PDA in sandwich mode, i.e., SERS from the Ag@PDA@Au_c-Ag_s assembly in different time domains, which has been achieved through in situ monitoring of incubation time of the Ag@PDA assembly in Au_c-Ag_s sol: (a) 6 h incubation; (b) 8 h incubation; (c) 10 h incubation; (d) 12 h incubation; (e) 14 h incubation; and (f) 16 h incubation. The spectral profiles clearly depict successive increases in the "hot-spot" areas through the augmented assembly of the Au_c-Ag_s particles over Ag@PDA which ultimately results in making the electromagnetic field effect more prominent with time.

strategy provides a "hot" site for SERS,[55] and when PDA molecules are locked in this nanogap, there is a giant contribution from the electromagnetic field effect which results in greatly enhanced SERS signals. From TEM images of the as-synthesized Ag nanoparticles we clearly observed that maximum numbers of particles have diameters of ∼50 nm, although it ranges from 20 to 50 nm. From the image it is also clearly understood that most of the particles coalesce with each other. This aggregation behavior has also been noticed in the FESEM and AFM analyses of the as-synthesized silver film. This feature leads to increasing numbers of "hot-spots" and makes the film SERS active. Therefore, the relatively large particle size with aggregation aspect/behavior also contributes

dx.doi.org/10.1021/jp5111955 | J. Phys. Chem. C XXXX, XXX, XXX−XXX

to the observed overall SERS enhancement in the sandwich mode (i.e., in Ag@PDA@Au_c-Ag_s).

Figure 3 presents the time-resolved SERS spectra from the Ag@PDA@Au_c-Ag_s assembly. This has been achieved through in situ monitoring of incubation time of the Ag@PDA assembly in Au_c-Ag_s sol [(Figure 3a) 6 h incubation; (Figure 3b) 8 h incubation; (Figure 3c) 10 h incubation; (Figure 3d) 12 h incubation; (Figure 3e) 14 h incubation; (Figure 3f) 16 h incubation]. The figure clearly presents the steady increase of totally symmetric vibrational modes of PDA with time with a subsequent reduction in intensities of the not totally symmetric modes. For example, the enhanced signal at 1444 cm^{-1} (Figure 3a; not totally symmetric mode) gradually decreases in intensity while the 1618 cm^{-1} band becomes prominent (Figure 3f; in-plane totally symmetric mode) with time. Similar situations arise for other modes also. This observation indicates a greater contribution from the electromagnetic field over chemical enhancement to the SERS of PDA molecules when we allowed longer incubation time. Therefore, it is envisaged that there are successive increases in "hot-spot" areas through the augmented assembly of Au_c-Ag_s particles over the Ag@PDA, which ultimately results in a more prominent electromagnetic field effect as time progresses. Thus, the above kinetics, measured in different time domains, enabled the assessment of the relative contributions of EM and CE characteristics in the SERS from Ag@PDA@Au_c-Ag_s entity.

It has been shown in different SERS studies through both experiment and simulation (like FDTD simulation) that effective EM field effect is more pronounced for Au_c-Ag_s particles in comparison to Ag particles only.[56] Thus, we have employed Ag sol in lieu of Au_c-Ag_s sol to introduce attachment of only Ag particles over Ag@PDA assembly in a second set of experiments. We then have the Ag@PDA@Ag assembly for recording SERS data. Figure 4 presents the SERS spectrum

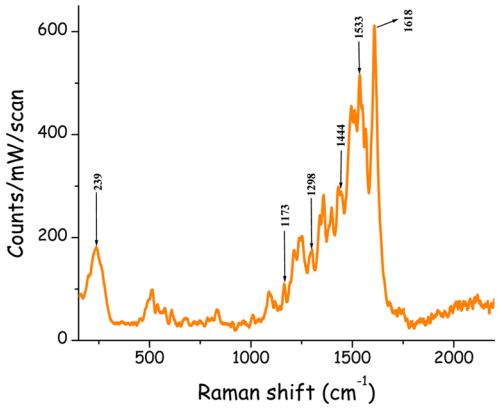

Figure 4. SERS spectrum of PDA (10^{-6} M) in altered sandwich mode where the molecule remains trapped in between the silver film and silver nanoparticles (i.e., SERS from Ag@PDA@Ag assembly).

from this assembly. Here also the highest intensity signal appears at 1618 cm^{-1} though the band is much less enhanced compared to previous examples (i.e., Ag@PDA@Au_c-Ag_s case). Other common bands are also observed (at 1533, 1444, 1173 cm^{-1}) but have very low intensity. Therefore, we can conclude that the contributions of EM and CE effects in SERS enhancement of PDA are smaller for Ag@PDA@Ag assembly compared to that of Ag@PDA@Au_c-Ag_s.

Our other set of SERS experiment with PDA anchored to only Au_c-Ag_s particles (i.e., no sandwich assembly) is shown in Supporting Information Figure S3 where we observe vibrational signatures of the molecules which are more allied with the SERS spectrum of the molecule over silver film (i.e., Figure 2b). However, the less intense spectral features indicate the lower contributions of EM and CE effects in the observed SERS with Au_c-Ag_s substrate compared to that of the Ag@PDA@Au_c-Ag_s sandwich substrate.

We then replaced the nanostructured silver film with a mechanically polished, thoroughly washed and cleaned silver foil and carry out SERS measurements with Ag-foil@PDA and Ag-foil@PDA@Au_c-Ag_s assemblies. Figure 5 presents the two

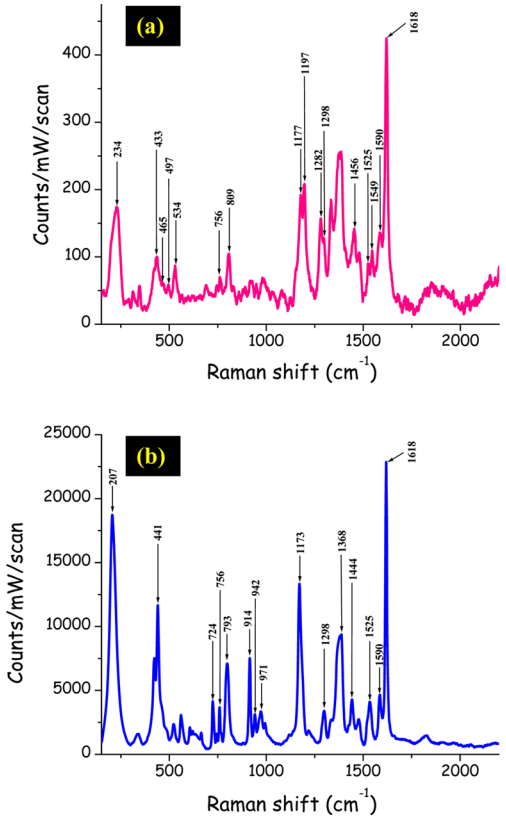

Figure 5. SERS spectrum of PDA (10^{-6} M) (a) on the cleaned silver foil (i.e., SERS from Ag-foil@PDA) and (b) in sandwich mode, i.e., when the molecule PDA remains trapped in between the silver foil and gold core−silver shell nanoparticles (i.e., SERS from Ag-foil@PDA@Au_c-Ag_s assembly).

spectra from these assemblies. We observed Raman signals of the PDA molecules when anchored over Ag foil (Figure 5a) though the spectral profile suffers from low intensity values. We then incubated the Ag-foil@PDA assembly in Au_c-Ag_s sol to configure the sandwich structure (i.e., Ag-foil@PDA@Au_c-Ag_s) like before. Figure 5b presents the SERS spectrum of PDA from Ag-foil@PDA@Au_c-Ag_s. Here it is worth mentioning that this SERS spectrum exactly resembles the SERS from Ag@PDA@Au_c-Ag_s but is again limited by its comparatively lower intensity. Here (i.e., for Ag-foil) the vibrational bands appear caused by the electromagnetic coupling of the localized surface plasmon of Au_c-Ag_s with the surface plasmon polariton of the underlying Ag foil, whereas for Ag@PDA@Au_c-Ag_s, the coupling occurs between the surface plasmons of the nanostructured Ag island and Au_c-Ag_s particles. The results establish that the latter coupling produces a greatly enhanced electromagnetic field in the nanogap of the sandwich structure, which in turn helps the

dx.doi.org/10.1021/jp5111955 | J. Phys. Chem. C XXXX, XXX, XXX−XXX

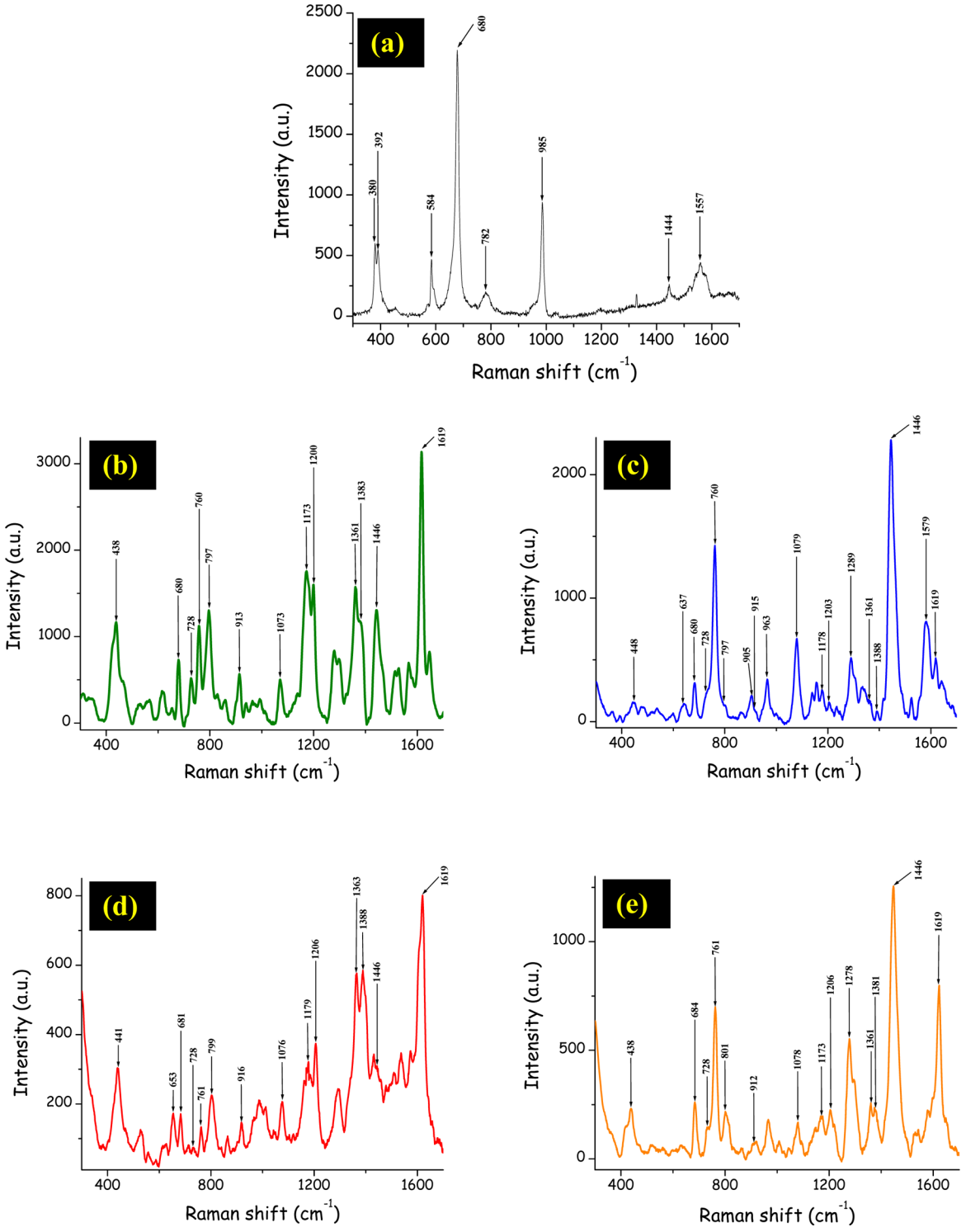

Figure 6. (a) NRS spectrum of solid melamine. (b–e) Concentration dependent SERS profiles of melamine in sandwich mode, i.e., when melamine remains trapped in between the nanostructured silver film deposited on the glass substrate and gold core–silver shell nanoparticles (i.e., concentration dependent SERS of melamine from nanostructured Ag-film@melamine@Au_c-Ag_s assembly). The presence of different marker bands (e.g., at ~680 cm^{-1}, 1078 cm^{-1}, 1446 cm^{-1}) even at 10^{-15} M concentration advocates the detection of melamine at the femtomolar level by this sandwich strategy. [Conditions: (b) 10^{-5} M; (c) 10^{-8} M; (d) 10^{-10} M; and (e) 10^{-15} M.]

PDA molecules show better SERS profile when it remains sandwiched between nanostructured Ag film and Au_c-Ag_s particles compared to the Ag-foil and Au_c-Ag_s particles.

We have also carried out the SERS study of the sandwich substrate (i.e., Ag@PDA@Au_c-Ag_s) using a 514 nm laser (Supporting Information Figure S4) as the excitation wavelength. As observed from Supporting Information Figure S4, less intense as well as poorly resolved spectral profiles are obtained from PDA in this excitation. Also, there is considerable overlap of different bands and the different bands are not distinctly observed like before (Figure 2c). Therefore, 632.8 nm irradiation was more effective than 514

dx.doi.org/10.1021/jp5111955 | J. Phys. Chem. C XXXX, XXX, XXX–XXX

nm in getting greatly enhanced SERS signals from the molecule, PDA, in the sandwich arrangement.

Thus, the above sets of experimental results clearly indicate that the hot spots produced in the nanogaps, formed between the nano Ag island and Au_c-Ag_s nanoparticles, are the essential sites for getting prolific SERS enhancement from a linker molecule, PDA, with 632.8 nm excitation. The superior enhancement results from the gigantic contribution from the electromagnetic field generated in the nanogaps of the sandwich structure. In a true sense, both CE and EM effects are responsible for SERS enhancement and any attempt to separate them would probably fail in one or more limits.

Detection of Femtomolar Concentration of Melamine. Finally the sandwich strategy was applied for the low level detection of melamine. To perform this, melamine was selected as the Raman probe in place of PDA. The SERS study was performed with four different concentrations of melamine (10^{-5}, 10^{-8}, 10^{-10}, and 10^{-15} M). For each case, we first fabricated the silver film over the glass slide, then incubated the film in melamine solution, followed by further incubation of the melamine anchored film in the gold core−silver shell colloid. Finally, we recorded the SERS spectra for all four sets and assigned all the peaks of melamine. Thus, Ag@melamine@Au_c-Ag_s assembly was fabricated and applied to the SERS study of melamine.

As reported in all the literature dealing with the SERS of melamine, the Raman signal at ∼680 cm^{-1} (calculated frequency ∼645 cm^{-1}) in the SERS profile could be considered the "fingerprint band". This band is assigned to the "ring breathing II" mode and involves an in-plane deformation of the triazine ring[37] of the molecule. Similarly, the band at ∼985 cm^{-1} ("ring breathing I" mode of the triazine ring) is also an in-plane vibrational mode. These bands are significantly enhanced when the molecule acquires a perpendicular orientation with respect to the surface of the adsorbate.[57] Similar conclusions could be made for the other ring breathing modes at ∼637 and ∼915 cm^{-1}, which also involve in-plane deformation of the triazine ring.

Figure 6 presents the NRS as well as the concentration dependent SERS spectra of melamine. Here it is also important to note that the SERS spectra of melamine, represented in the above figure, have intensity profiles in the arbitrary units. We also noticed that the intensity profiles for different bands subsequently vary from each other in the above spectra.

In the SERS spectra, the vibrational bands are distinctly observed. The most recognized ∼680 cm^{-1} band is observed in the SERS spectra for all concentrations. Other significantly enhanced SERS signals appear at ∼730, ∼760, and ∼800 cm^{-1}, which are observed in the SERS spectra for all the concentrations. The ring-stretching vibrations emerge at ∼1068 and ∼1078 cm^{-1}. These bands belong to out-of-plane modes. The distinct 1446 cm^{-1} band could be assigned to the semicircle ring stretching mode. The bands appearing in the 1500−1600 cm^{-1} wavenumber region, such as the bands observed at ∼1530 and ∼1580 cm^{-1}, belong to the quadrant ring stretching vibrations. Another vibrational band is observed at ∼1619 cm^{-1} for all the concentrations which arises from the NH_2 deformation mode of melamine. Here it is worth noting that the observed spectroscopic features of melamine in our case appear identical to the SERS spectrum of melamine from vertical gold nanorod arrays reported by Xiong et al.[46] The vibrational features therefore are not background signals from the substrate itself and truly present the correct SERS profiles of melamine.

This spectral observation in our case suggests a prime contribution of the CE effect along with EM effect in the observed SERS enhancement of melamine. Though in the case of PDA, we have observed giant enhancement (i.e., higher EM effect) of the totally symmetric modes when the molecules are located in the nanogap of the sandwich structure, in the case of melamine, the out-of-plane modes are more significantly enhanced (i.e., higher CE effect) over the in-plane modes. This presumably results from the superior binding capability of melamine to the available metal surface through its large number of binding sites. Finally, with this strategy we were able to detect melamine concentration down to the femtomolar level (i.e., limit of detection = 10^{-15} M).[27−46] In this study, our main aim was to fabricate a new SERS active nanodimensional architecture as a deliverable for field application. Therefore, the as-obtained accurate SERS spectra of melamine even in femtomolar (10^{-15} M) concentration clearly indicate that our sandwich-based SERS strategy is truly successful to present correct and reproducible vibrational information from a SERS active molecule, melamine.

CONCLUSIONS

In conclusion, our present effort describes a modified sandwich-based SERS recipe to achieve prolific SERS enhancement from selected Raman probes. The strategy involves fabrication of a nanostructured silver film on a glass slide employing a simple colloidal chemistry approach followed by anchoring of a Raman active linker molecule (here we have chosen *para*-phenylenediamine or PDA) on the nanoparticles and, finally, further attachment of Au_c-Ag_s nanoparticles on the molecule. The two amino groups at C-1 and C-4 of the PDA molecule could simultaneously attach onto the Ag and Au_c-Ag_s nanoparticle surface and therefore remain trapped between these two plasmonic nanostructures in a sandwich fashion. SERS study was carried out on this "nanostructured Ag-film @PDA@Au_c-Ag_s" assembly. Comparative SERS studies were also performed on this molecule in other plasmonic environments as described in the above discussion. From all the SERS performances of PDA in the different conditions, we conclude that maximum SERS enhancement could be achieved by employing the sandwich arrangement of nanostructured Ag@PDA@Au_c-Ag_s. Here, the spectral bands are also discrete in nature and well resolved. It is believed that the large number of SERS active hot-spots, produced in the nanogaps between nanostructured Ag film and Au_c-Ag_s nanoparticles, result in an exceedingly enhanced electromagnetic field. The superior enhancement of Raman signals in the above sandwich mode thus results from the gigantic contribution from this electromagnetic field generated in the above nanogaps through coupling of the localized surface plasmons of the nanostructured metals/metal nanoparticles. Finally, we have employed this SERS active sandwich-based plasmonic platform for the analytical assay of melamine. Four individual SERS measurements were carried out with four different concentrations of melamine. Enormous SERS enhancement has also been achieved from this molecule. Ultimately, with this strategy we were able to detect melamine concentration down to the femtomolar (10^{-15} M) level. Thus, our newly designed SERS active sandwich platform offers great promise toward trace level detection of melamine. Finally, we strongly believe that this modified sandwich-based SERS protocol could be an advanced avenue for low level

dx.doi.org/10.1021/jp5111955 | J. Phys. Chem. C XXXX, XXX, XXX−XXX

determination/detection of other different contaminants (e.g., food adulterants, pesticides, drugs, pollutants) in a simple and time-saving way.

■ ASSOCIATED CONTENT

Supporting Information

Analytical methods; characterizations of the Au_c-Ag_s nanoparticles (Figure S1); EDX pattern and elemental mapping analysis of the nanostructured silver film (Figure S2); SERS spectrum of PDA (10^{-6} M) over only Au_c-Ag_s nanoparticles (Figure S3); SERS spectrum of PDA in sandwich mode using 514 nm laser excitation source (Figure S4). This material is available free of charge via the Internet at http://pubs.acs.org..

■ AUTHOR INFORMATION

Corresponding Author

*E-mail: tpal@chem.iitkgp.ernet.in.

Notes

The authors declare no competing financial interest.

■ ACKNOWLEDGMENTS

The authors are thankful to the CSIR, UGC, DST, and Indian Institute of Technology, Kharagpur for financial assistance.

■ REFERENCES

(1) Fleischman, M.; Hendra, P. J.; McQuillan, A. J. Raman Spectra of Pyridine Adsorbed at a Silver Electrode. *Chem. Phys. Lett.* **1974**, *26*, 163−166.

(2) Jeanmaire, D. J.; Van Duyne, R. P. Surface Raman Spectroelectrochemistry: Heterocyclic, Aromatic, and Aliphatic Amines Adsorbed on the Anodized Silver Electrode. *J. Electroanal. Chem.* **1977**, *84*, 1−20.

(3) Albrecht, M. G.; Creighton, J. A. Anomalously Intense Raman Spectra of Pyridine at a Silver Electrode. *J. Am. Chem. Soc.* **1977**, *99*, 5215−5217.

(4) Brown, R. J. C.; Milton, M. J. T. Nanostructures and Nanostructured Substrates for Surface Enhanced Raman Scattering (SERS). *J. Raman Spectrosc.* **2008**, *39*, 1313−1326.

(5) Tian, Z.-Q.; Ren, B.; Wu, D.-Y. Surface Enhanced Raman Scattering: From Noble to Transition Metals and from Rough Surfaces to Ordered Nanostructures. *J. Phys. Chem. B* **2002**, *106*, 9463−9483.

(6) Sarkar, S.; Pradhan, M.; Sinha, A. K.; Basu, M.; Pal, T. Chelate Effect in Surface Enhanced Raman Scattering with Transition Metal Nanoparticles. *J. Phys. Chem. Lett.* **2010**, *1*, 439−444.

(7) Wei, W.; Li, S.; Millstone, J. E.; Banholzer, M. J.; Chen, X.; Xu, X.; Schatz, G. C.; Mirkin, C. A. Surprisingly Long-Range Surface-Enhanced Raman Scattering (SERS) on Au−Ni Multisegmented Nanowires. *Angew. Chem., Int. Ed.* **2009**, *48*, 4210−4212.

(8) Sajanlal, P. R.; Pradeep, T. Functional Hybrid Nickel Nanostructures as Recyclable SERS Substrates: Detection of Explosives and Biowarfare Agents. *Nanoscale* **2012**, *4*, 3427−3437.

(9) Wang, Y.; Zou, X.; Ren, W.; Wang, W.; Wang, E. Effect of Silver Nanoplates on Raman Spectra of *p*-Aminothiophenol Assembled on Smooth Macroscopic Gold and Silver Surface. *J. Phys. Chem. C* **2007**, *111*, 3259−3265.

(10) Orendorff, C. J.; Gole, A.; Sau, T. K.; Murphy, C. J. Surface Enhanced Raman Spectroscopy of Self-Assembled Monolayers: Sandwich Architecture and Nanoparticle Shape Dependence. *Anal. Chem.* **2005**, *77*, 3261−3266.

(11) Gaudig, T. D.; Rauls, E.; Deckert, V. Aromatic Amino Acid Monolayers Sandwiched between Gold and Silver: A Combined Tip-Enhanced Raman and Theoretical Approach. *J. Phys. Chem. C* **2010**, *114*, 7412−7420.

(12) Pavel, I.; McCarney, E.; Elkhaled, A.; Morrill, A.; Plaxco, K.; Moskovits, M. Label Free SERS Detection of Small Proteins Modified to Act as Bifunctional Linkers. *J. Phys. Chem. C* **2008**, *112*, 4880−4883.

(13) Han, X. X.; Kitahama, Y.; Itoh, T.; Wang, C. X.; Zhao, B.; Ozaki, Y. Protein-Mediated Sandwich Strategy for Surface-Enhanced Raman Scattering: Application to Versatile Protein Detection. *Anal. Chem.* **2009**, *81*, 3350−3355.

(14) Kim, K.; Shin, D.; Kim, L. K.; Shin, K. S. Electromagnetic Field Enhancement in the Gap between Two Au Nanoparticles: The Size of Hot Site Probed by Surface Enhanced Raman Scattering. *Phys. Chem. Chem. Phys.* **2010**, *12*, 3747−3752.

(15) Kim, K.; Choi, J.-Y.; Lee, H. B.; Shin, K. S. Raman Scattering of 4-Aminobenzenethiol Sandwiched between Ag Nanoparticle and Macroscopically Smooth Au Substrate: Effects of Size of Ag Nanoparticles and the Excitation Wavelength. *J. Chem. Phys.* **2011**, *135*, 124705−124713.

(16) Kim, K.; Lee, H. B.; Choi, J.-Y.; Kim, L. K.; Shin, K. S. Surface-Enhanced Raman Scattering of 4-Aminobenzenethiol in Nanogaps between a Planar Ag Substrate and Pt Nanoparticles. *J. Phys. Chem. C* **2011**, *115*, 13223−13231.

(17) Kim, K.; Lee, H. B.; Choi, J.-Y.; Shin, K. S. Characteristics of Nanogaps Formed by Planar Au and Pt Nanoparticles Revealed by Raman Spectroscopy. *J. Phys. Chem. C* **2011**, *115*, 21047−21055.

(18) Kim, K.; Lee, H. B.; Yoon, J. K.; Shin, D.; Shin, K. S. Ag Nanoparticle-Mediated Raman Scattering of 4-Aminobenzenethiol on a Pt Substrate. *J. Phys. Chem. C* **2010**, *114*, 13589−13595.

(19) Yoon, J. K.; Kim, K.; Shin, K. S. Raman Scattering of 4-Aminobenzenethiol Sandwiched between Au Nanoparticles and a Macroscopically Smooth Au Substrate: Effect of Size of Au Nanoparticles. *J. Phys. Chem. C* **2009**, *113*, 1769−1774.

(20) Kim, K.; Choi, J.-Y.; Shin, K. S. Enhanced Raman Scattering in Gaps Formed by Planar Au and Au/Ag Alloy Nanoparticles. *J. Phys. Chem. C* **2013**, *117*, 11421−11427.

(21) Smith, W. E. Practical Understanding and Use of Surface Enhanced Raman Scattering/Surface Enhanced Resonance Raman Scattering in Chemical and Biological Analysis. *Chem. Soc. Rev.* **2008**, *37*, 955−964 and references therein..

(22) Graham, D.; Goodacre, R. Chemical and Bioanalytical Applications of Surface Enhanced Raman Scattering Spectroscopy. *Chem. Soc. Rev.* **2008**, *37*, 883−884.

(23) Porter, M. D.; Lipert, R. J.; Siperko, L. M.; Wang, G.; Narayanan, R. SERS as a Bioassay Platform: Fundamentals, Design, and Applications. *Chem. Soc. Rev.* **2008**, *37*, 1001−1011 and references therein..

(24) Wang, Y.; Polavarapu, L.; Liz-Marzán, L. M. Reduced Graphene Oxide-Supported Gold Nanostars for Improved SERS Sensing and Drug Delivery. *ACS Appl. Mater. Interfaces* [Online early access] DOI: 10.1021/am501382y. Published online May 14, 2014.

(25) Alvarez-Puebla, R. A.; Liz-Marzán, L. M. SERS Detection of Small Inorganic Molecules and Ions. *Angew. Chem., Int. Ed.* **2012**, *51*, 11214−11223 and references therein..

(26) Saha, A.; Jana, N. R. Detection of Cellular Glutathione and Oxidized Glutathione Using Magnetic-Plasmonic Nanocomposite-Based "Turn-Off" Surface Enhanced Raman Scattering. *Anal. Chem.* **2013**, *85*, 9221−9228.

(27) Yue, J.; Jiang, X.; Kaneti, Y. V.; Yu, A. Deposition of Gold Nanoparticles on β-FeOOH Nanorods for Detecting Melamine in Aqueous Solution. *J. Colloid Interface Sci.* **2012**, *367*, 204−212.

(28) Ma, Y.; Jiang, L.; Mei, Y.; Song, R.; Tian, D.; Huang, H. Colorimetric Sensing Strategy for Mercury(II) and Melamine Utilizing Cysteamine-modified Gold Nanoparticles. *Analyst* **2013**, *138*, 5338−5343.

(29) Ma, Y.; Niu, H.; Zhang, X.; Cai, Y. One-Step Synthesis of Silver/Dopamine Nanoparticles and Visual Detection of Melamine in Raw Milk. *Analyst* **2011**, *136*, 4192−4196.

(30) Fodey, T. L.; Thompson, C. S.; Traynor, I. M.; Haughey, S. A.; Kennedy, D. G.; Crooks, S. R. H. Development of an Optical Biosensor Based Immunoassay to Screen Infant Formula Milk Samples for Adulteration with Melamine. *Anal. Chem.* **2011**, *83*, 5012−5016.

(31) Sanji, T.; Nakamura, M.; Kawamata, S.; Tanaka, M.; Itagaki, S.; Gunji, T. Fluorescence "Turn-On" Detection of Melamine with

Aggregation-Induced-Emission-Active Tetraphenylethene. *Chem.—Eur. J.* **2012**, *18*, 15254−15257.
(32) Han, S.; Zhu, S.; Liu, Z.; Hu, L.; Parveen, S.; Xu, G. Oligonucleotide-Stabilized Fluorescent Silver Nanoclusters for Turn-on Detection of Melamine. *Biosens. Bioelectron.* **2012**, *36*, 267−270.
(33) Gao, F.; Ye, Q.; Cui, P.; Zhang, L. Efficient Fluorescence Energy Transfer System between CdTe-Doped Silica Nanoparticles and Gold Nanoparticles for Turn-On Fluorescence Detection of Melamine. *J. Agric. Food Chem.* **2012**, *60*, 4550−4558.
(34) Zhou, Q.; Liu, N.; Qie, Z.; Wang, Y.; Ning, B.; Gao, Z. Development of Gold Nanoparticle-Based Rapid Detection Kit for Melamine in Milk Products. *J. Agric. Food Chem.* **2011**, *59*, 12006−12011.
(35) Lee, J.; Jeong, E. J.; Kim, J. Selective and Sensitive Detection of Melamine by Intra/Inter Liposomal Interaction of Polydiacetylene Liposomes. *Chem. Commun.* **2011**, *47*, 358−360.
(36) Yang, S.; Ding, J.; Zheng, J.; Hu, B.; Li, J.; Chen, H.; Zhou, Z.; Qiao, X. Detection of Melamine in Milk Products by Surface Desorption Atmospheric Pressure Chemical Ionization Mass Spectrometry. *Anal. Chem.* **2009**, *81*, 2426−2436.
(37) Zhang, X.-F.; Zou, M.-Q.; Qi, X.-H.; Liu, F.; Zhu, X.-H.; Zhao, B. −H Detection of Melamine in Liquid Milk using Surface Enhanced Raman Scattering Spectroscopy. *J. Raman Spectrosc.* **2010**, *41*, 1655−1660.
(38) Wen, Z. Q.; Li, G.; Ren, D. Detection of Trace Melamine in Raw Materials used for Protein Pharmaceutical Manufacturing Using Surface Enhanced Raman Spectroscopy (SERS) with Gold Nanoparticles. *Appl. Spectrosc.* **2011**, *65*, 514−521.
(39) Kämmer, E.; Dörfer, T.; Csáki, A.; Schumacher, W.; Filho, P. A. D. C.; Tarcea, N.; Fritzsche, W.; Rösch, P.; Schimtt, M.; Popp, J. Evaluation of Colloids and Activation Agents for Determination of Melamine Using UV-SERS. *J. Phys. Chem. C* **2012**, *116*, 6083−6091.
(40) Betz, J. F.; Cheng, Y.; Rubloff, G. W. Direct SERS Detection of Contaminants in A Complex Mixture: Rapid, Single Step Screening for Melamine in Liquid Infant Formula. *Analyst* **2012**, *137*, 826−828.
(41) Chen, L.-M.; Liu, Y.-N. Surface-Enhanced Raman Detection of Melamine on Silver-Nanoparticle-Decorated Silver/Carbon Nanospheres: Effect of Metal Ions. *ACS Appl. Mater. Interfaces* **2011**, *3*, 3091−3096.
(42) Hu, H.; Wang, Z.; Pan, L.; Zhao, S.; Zhu, S. Ag-Coated Fe_3O_4@SiO_2 Three-Ply Composite Microspheres: Synthesis, Characterization, and Application in Detecting Melamine with Their Surface-Enhanced Raman Scattering. *J. Phys. Chem. C* **2010**, *114*, 7738−7742.
(43) Koglin, E.; Kip, B. J.; Meier, R. J. Adsorption and Displacement of Melamine at the Ag/Electrolyte Interface Probed by Surface-Enhanced Raman Microprobe Spectroscopy. *J. Phys. Chem. C* **1996**, *100*, 5078−5089.
(44) Li, J.-M.; Ma, W.-F.; Wei, C.; You, L.-J.; Guo, J.; Hu, J.; Wang, C.-C. Detecting Trace Melamine in Solution by SERS Using Ag Nanoparticle Coated Poly(styrene-co-acrylic acid) Nanospheres as Novel Active Substrates. *Langmuir* **2011**, *27*, 14539−14544.
(45) White, I. M.; Yazdi, S. H. Optofluidic Surface Enhanced Raman Spectroscopy Microsystem for Sensitive and Repeatable On-Site Detection of Chemical Contaminants. *Anal. Chem.* **2012**, *84*, 7992−7998.
(46) Peng, B.; Li, G.; Li, D.; Dodson, S.; Zhang, Q.; Zhang, J.; Lee, Y. H.; Demir, H. V.; Ling, X. Y.; Xiong, Q. *ACS Nano* **2013**, *7*, 5993−6000.
(47) Rodríguez-González, B.; Burrows, A.; Watanabe, M.; Kiely, C. J.; Liz-Marzán, L. M. Multishell Bimetallic AuAg Nanoparticles: Synthesis, Structure and Optical Properties. *J. Mater. Chem.* **2005**, *15*, 1755−1759.
(48) Frens, G. *Nat. Phys. Sci.* **1973**, *241*, 20−22.
(49) Dutta, S.; Sarkar, S.; Ray, C.; Roy, A.; Sahoo, R.; Pal, T. Mesoporous Gold and Palladium Nanoleaves from Liquid−Liquid Interface: Enhanced Catalytic Activity of the Palladium Analogue toward Hydrazine-Assisted Room-Temperature 4-Nitrophenol Reduction. *ACS Appl. Mater. Interfaces* **2014**, *6*, 9134−9143.
(50) Sau, T. K.; Pal, A.; Pal, T. Size Regime Dependent Catalysis by Gold Nanoparticles for the Reduction of Eosin. *J. Phys. Chem. B* **2001**, *105*, 9266−9272.
(51) Chandra, S.; Chowdhury, J.; Ghosh, M.; Talapatra, G. B. Genesis of Enhanced Raman Bands in SERS Spectra of 2-Mercaptoimidazole: FTIR, Raman, DFT, and SERS. *J. Phys. Chem. A* **2012**, *116*, 10934−10947.
(52) Chipman, D. M.; Sun, Q.; Tripathi, G. N. R. Para Phenylenediamine Radical Cation Structure Studied by Resonance Raman and Molecular Orbital Methods. *J. Chem. Phys.* **2011**, *135*, 124705−124713.
(53) Moskovits, M.; Suh, J. S. Surface Selection Rules for Surface-Enhanced Raman Spectroscopy: Calculations and Application to the Surface-Enhanced Raman Spectrum of Phthalazine on Silver. *J. Phys. Chem.* **1984**, *88*, 5526−5530.
(54) Creighton, J. A. Surface Raman Electromagnetic Enhancement Factors for Molecules at the Surface of Small Isolated Metal Spheres: The Determination of Adsorbate Orientation from SERS Relative Intensities. *Surf. Sci.* **1983**, *124*, 209−219.
(55) McMahon, J. M.; Li, S.; Ausman, L. K.; Schatz, G. C. Modeling the Effect of Small Gaps in Surface-Enhanced Raman Spectroscopy. *J. Phys. Chem. C* **2012**, *116*, 1627−1637.
(56) Pande, S.; Chowdhury, J.; Pal, T. Understanding the Enhancement Mechanisms in the Surface-Enhanced Raman Spectra of the 1,10-Phenanthroline Molecule Adsorbed on a Au@Ag Bimetallic Nanocolloid. *J. Phys. Chem. C* **2011**, *115*, 10497−10509.
(57) Otto, A. The 'Chemical' (Electronic) Contribution to Surface-Enhanced Raman Scattering. *J. Raman Spectrosc.* **2005**, *36*, 497−509.